A Shock Tube Study of $H_2 + OH \rightarrow H_2O + H$ Using OH Laser Absorption

KING-YIU LAM, DAVID F. DAVIDSON, RONALD K. HANSON

Department of Mechanical Engineering, Stanford University, Stanford, CA 94305

Received 27 September 2012; accepted 13 November 2012

DOI 10.1002/kin.20771
Published online 23 April 2013 in Wiley Online Library (wileyonlinelibrary.com).

ABSTRACT: The rate constant for the reaction of hydroxyl radicals (OH) with molecular hydrogen (H_2) was measured behind reflected shock waves using UV laser absorption of OH radicals near 306.69 nm. Test gas mixtures of H_2 and tert-butyl hydroperoxide (TBHP) diluted in argon were shock-heated to temperatures ranging from 902 to 1518 K at pressures of 1.15–1.52 atm. OH radicals were produced by rapid thermal decomposition of TBHP at high temperatures. The rate constant for the title reaction was inferred by best fitting the measured OH time histories with the simulated profiles from the comprehensive reaction mechanism of Wang et al. (USC-Mech v2.0) (2007). The measured values can be expressed in the Arrhenius equation as $k_1(T) = 4.38 \times 10^{13} \exp(-3518/T)$ cm^3 mol^{-1} s^{-1} over the temperature range studied. A detailed error analysis was performed to estimate the overall uncertainty of the title reaction, and the estimated ($2 - \sigma$) uncertainties were found to be ±17% at 972 and 1228 K. The present measurements are in excellent agreement with the previous experimental studies from Frank and Just (*Ber Bunsen-Ges Phys Chem* 1985, 89, 181–187), Michael and Sutherland (*J Phys Chem* 1988, 92, 3853–3857), Davidson et al. (*Symp (Int) Combust* 1988, 22, 1877–1885), Oldenborg et al. (*J Phys Chem* 1992, 96, 8426–8430), and Krasnoperov and Michael (*J Phys Chem A* 2004, 108, 5643–5648).In addition, the measured rate constant is in close accord with the non-Arrhenius expression from GRI-Mech 3.0 (http://www.me.berkeley.edu/gri_mech/) and the theoretical calculation using semiclassical transition state theory from Nguyen et al. (*Chem Phys Lett* 2010, 499, 9–15). © 2013 Wiley Periodicals, Inc. Int J Chem Kinet 45: 363–373, 2013

INTRODUCTION

The reaction of hydroxyl radicals with molecular hydrogen

$$H_2 + OH \rightarrow H_2O + H \qquad (1)$$

is an important chain-propagating reaction in hydrogen combustion. Its reverse reaction plays a critical role in the establishment of partial equilibrium in the postcombustion regime. In addition, owing to the large abundance of H_2 in the atmosphere, reaction (1) controls the atmospheric concentration of OH, which is a major tropospheric oxidizer. The increase in the atmospheric H_2 concentration (resulting from the combustion of fossil fuels and biomass) can significantly reduce the atmospheric OH concentration. Such reduction in the OH concentration will prolong the residence times of industrial and natural pollutants in the atmosphere, which can have a detrimental impact on the environment.

Correspondence to: King-Yiu Lam; e-mail: klam1@stanford.edu.

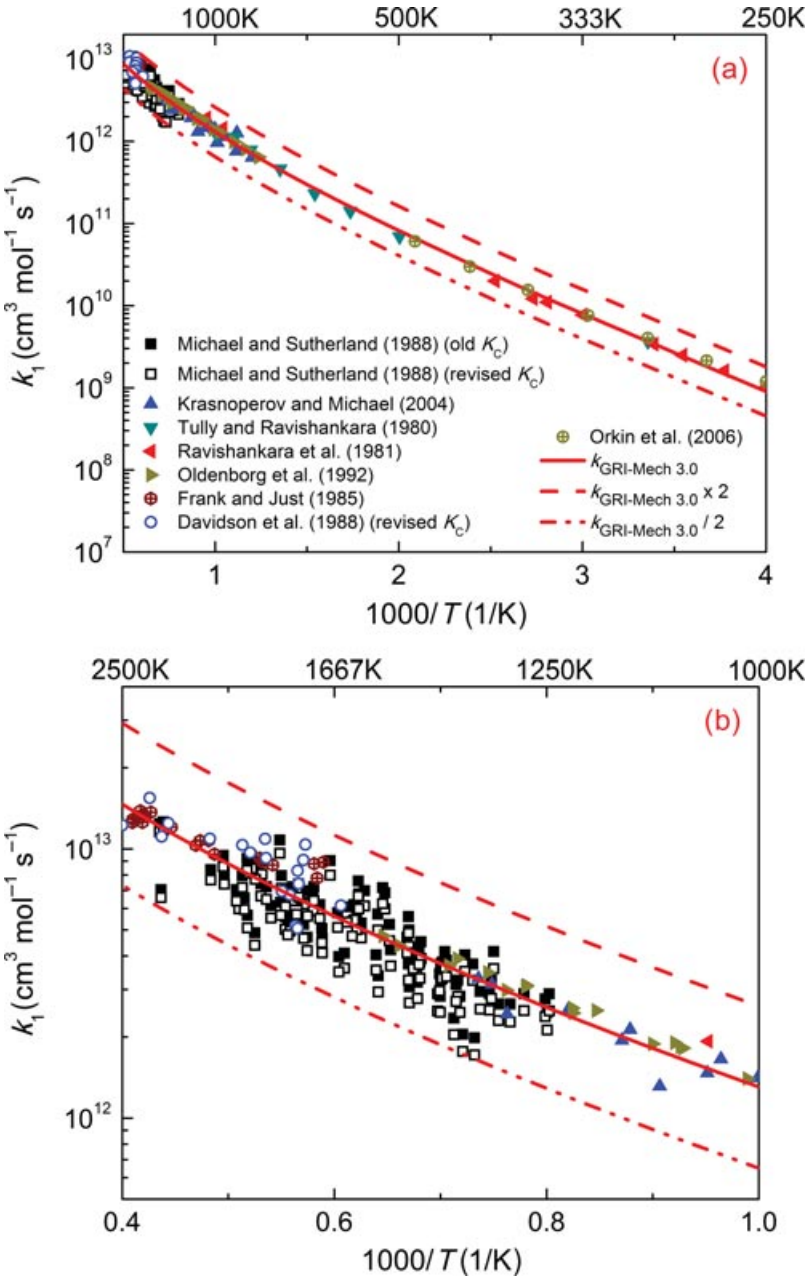

Figure 1 (a) Arrhenius plot for the reaction of OH with H_2 at all temperatures. (b) Arrhenius plot for the reaction of OH with H_2 at high temperatures (1000–2500 K).

Because of its important role in combustion and atmospheric chemistry, numerous direct rate constant measurements for reaction (1) have been conducted across a broad range of temperatures [1–20]. Figure 1 demonstrates some of the previous experimental determinations for reaction (1). Ravishankara and coworkers [7,8] measured the rate constant for the title reaction (under pseudo–first-order kinetic conditions) using the flash photolysis–resonance fluorescence technique to monitor the temporal profiles of OH decays in a heated quartz cell over 250–1050 K. Their measurements confirmed the nonlinearity of the Arrhenius plot for reaction (1) over this wide temperature range. Recently, Orkin et al. [14] reexamined the rate constant for reaction (1) using the flash photolysis–resonance fluorescence technique in a Pyrex reactor over a narrower temperature range of 200–479 K, and their results are in excellent agreement with the

measured values from Ravishankara and coworkers [7,8]. At combustion-relevant conditions ($T > 1000$ K), the measurements for reaction (1) were generally carried out using shock tubes and these high-temperature data have a much larger scatter (within a factor of 2) than the low-temperature data, as illustrated in Fig. 1. Frank and Just [16] measured the rate constants for the reactions of $H + O_2 \rightarrow OH + O$ and $H_2 + OH \rightarrow H_2O + H$ by employing atomic resonance absorption spectrometry (ARAS) to monitor H- and O-atom concentration profiles behind reflected shock waves over 1700–2500 K. Michael and Sutherland [17] studied the rate constant for the reaction of $H + H_2O \rightarrow H_2 + OH$ (reaction (–1)) using flash photolysis of H_2O to generate H-atoms and using ARAS to monitor the temporal profiles of H-atom decays behind reflected shock waves over 1246–2297 K. The rate constant for reaction (1) was calculated from the measured reverse rate constant and the equilibrium constant, and the resulting data were then compiled with the earlier experimental work from Ravishankara and coworkers [7,8] and Frank and Just [16] to form a three-parameter least-squares fit: $k_1(T) = 2.16 \times 10^8\ T^{1.51}$ exp(–3430 [cal/mol]/RT) cm^3 mol^{-1} s^{-1} over 250–2500 K. This expression is currently adopted in GRI-Mech 3.0 [21]. It is pertinent to note that the recent revised standard enthalpy of formation for OH at 298 K [22] seems to suggest a lower rate constant expression for reaction (1) (∼15% lower) if the rate constant is evaluated from the reverse reaction and the revised equilibrium constant. Figure 1 also shows the revised evaluations from Michael and Sutherland [17] using the revised equilibrium constants. Similarly, Davidson et al. [18] studied the rate constant for the reverse reaction by using laser photolysis of H_2O and UV laser absorption of OH near 307 nm behind reflected shock waves over 1600–2500 K and the rate constant for reaction (1) can be evaluated from their measured values and the revised equilibrium constants, as shown in Fig. 1. Oldenborg et al. [19] conducted direct rate constant measurements for reaction (1) (under pseudo–first-order kinetic conditions) using the laser photolysis/laser-induced fluorescence technique to monitor OH radical concentration profiles in a heated cell over 800–1550 K. Moreover, Krasnoperov and Michael [20] reexamined the rate constant for reaction (1) using a novel multipass absorption spectrometric detection technique to monitor OH species profiles at 308 nm in reflected shock wave experiments over 832–1359 K.

An accurate knowledge of the rate constant for reaction (1) is important in interpreting laminar flame speed measurements of H_2–O_2 mixtures. Figure 2 presents the unstretched laminar flame speed measurements of H_2–air mixtures as a function of the equivalence ratio at standard initial temperature (298 K) and ambient pressure (1 atm) [23–30], along with the simulations from the preliminary CEFRC (Combustion Energy Frontier Research Center) foundational fuel model [31]. Note that the previous rate constant measurements of reaction (1) have a relatively large scatter (within a factor

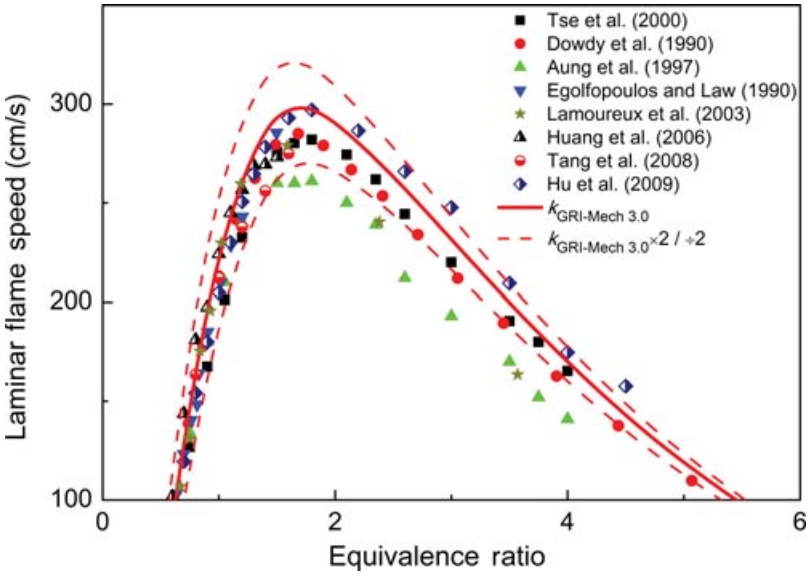

Figure 2 Impact of the rate constant for the reaction of $H_2 + OH \rightarrow H_2O + H$ on the laminar flame speed predictions of H_2–air mixtures at 298 K and 1 atm. Laminar flame speed simulations were performed using the preliminary CEFRC foundational fuel model [31].

of 2) at elevated temperatures, and such large uncertainty in reaction (1) can affect the laminar flame speed predictions of H_2–air mixtures from the model by approximately ±11%, as demonstrated in Fig. 2. Thus, there is motivation to reduce the existing experimental uncertainty in k_1 at combustion-relevant conditions. In the present study, we aim to report the rate constant for the title reaction with a much lower experimental scatter and overall uncertainty over the temperature range of 902–1518 K.

EXPERIMENTAL

Experiments were performed in a stainless steel, high-purity, low-pressure shock tube at Stanford. The shock tube is composed of a 3.7-m driver section and a 10-m driven section, with an inner diameter of 15.24 cm. Reflected shock temperatures and pressures were determined from the incident shock speed at the endwall using standard normal shock relations, with uncertainties of approximately ±0.7% and ±1%, respectively, mainly due to the uncertainty in the measured shock velocity (±0.2%). The endwall incident shock speed was measured using a series of five piezoelectric pressure transducers over the last 1.5 m of the shock tube and linearly extrapolated to the endwall. The OH laser diagnostic, along with a Kistler™ piezoelectric pressure transducer for pressure measurements, was located at a test section 2 cm from the driven section endwall.

Between experiments, the shock tube and mixing assembly were routinely turbomolecular pumped down to ∼5 μTorr to ensure purity of the test mixtures. Test mixtures were prepared manometrically in a 40-L stainless-steel tank heated uniformly to 50°C and mixed with a magnetically driven stirring vane. A double-dilution process was employed to allow for more accurate pressure measurements in the manometrical preparation of a highly dilute mixture. A highly concentrated mixture was first prepared and mixed for at least 2 h to ensure homogeneity and consistency, and the mixture was then further diluted with argon and mixed for additional 2 h prior to the experiments. The gases utilized in this study were hydrogen (research grade) 99.999% and argon (research grade) 99.999%, which were supplied by Praxair and used without further purification. The liquid chemical was commercially available 70% tert-butyl hydroperoxide (TBHP) in water from Sigma-Aldrich (Milwaukee, WI, USA) and was purified using a freeze–pump–thaw procedure to remove dissolved volatiles and air prior to mixture preparation.

The OH radical concentration was measured using the frequency-doubled output of a narrow-linewidth ring dye laser near 306.69 nm. The laser wavelength was tuned to the peak of the well-characterized $R_1(5)$ absorption line in the OH A–X (0, 0) band. Visible light near 613.4 nm was generated by pumping Rhodamine 6G dye in a Spectra Physics 380A laser cavity with the 5-W, cw output of a Coherent Verdi laser at 532 nm. The visible light was then intracavity frequency-doubled using a temperature-tuned AD*A nonlinear crystal to generate ∼1 mW of light near 306.69 nm. Using a common-mode-rejection detection scheme, a minimum absorbance of 0.1% could be detected, which resulted in a minimum detection sensitivity of ∼0.2 ppm at 1400 K and 1.5 atm. Further details of the OH laser diagnostic setup are discussed elsewhere [22,32]. The OH radical concentration can be calculated from Beer's law: $I/I_o = \exp(-k_{OH}X_{OH}PL)$, where I and I_o are the transmitted and incident laser intensities, k_{OH} is the OH absorption coefficient, X_{OH} is the OH mole fraction, P is the total pressure, and L is the path length (15.24 cm). The overall estimated uncertainty in the measured OH mole fraction (X_{OH}) is approximately ±3%, mainly due to the uncertainty in temperature (±0.7%). Measurements were also conducted with the laser tuned away from the absorption line to verify that there was no significant interference absorption or emission. All data were recorded at 2 MHz using a high-resolution (14 bit) data acquisition system.

KINETIC MEASUREMENTS

A series of 21 reflected shock wave experiments were conducted to determine the rate constant for the reaction of $H_2 + OH \rightarrow H_2O + H$ over the temperature range of 902–1518 K at pressures of 1.15–1.52 atm. Dilute test mixtures with 94–125 ppm TBHP (and water) and 1001–1516 ppm H_2 in argon were used to minimize the temperature drop caused by the chemistry effects, and the temperature profile behind the reflected shock wave was nearly constant (<1 K change) over the time frame of the experiment. In the present study, the CHEMKIN PRO package [33] was used to simulate the consumption of OH radicals by molecular hydrogen under the standard constant energy and volume assumption and a comprehensive reaction mechanism of Wang et al. (USC-Mech v2.0) [34] was selected as the base mechanism. This mechanism consists of 111 species and 784 elementary reactions and has been validated against a series of shock tube ignition delay times, laminar flame speeds, and speciation data from a shock tube and a flow reactor during high-temperature oxidation of H_2, CO, and C1–C4 hydrocarbons. It is pertinent to note that the conclusions of the present

Table I Reactions Describing $H_2 + OH$ Experiments at P = 1.3 atm

Reaction	Rate Constant ($cm^3\ mol^{-1}\ s^{-1}$)			Number	Reference
	A	*b*	*E* (cal/mol)		
$H_2 + OH \rightarrow H_2O + H$		See the text		1	This work
$TBHP \rightarrow (CH_3)_3CO + OH$	3.57E+13	0	3.575E+04	2	[36]
$(CH_3)_3CO \rightarrow CH_3COCH_3 + CH_3$	1.26E+14	0	1.530E+04	3	[37]
$TBHP + OH \rightarrow H_2O + O_2 + \text{tert-}C_4H_9$	2.30E+13	0	5.223E+03	4	[36]
$TBHP + OH \rightarrow H_2O + HO_2 + \text{iso-}C_4H_8$	2.49E+13	0	2.655E+03	5	[36]
$CH_3 + OH \rightarrow CH_2(s) + H_2O$	1.65E+13	0	0	6	[36]
$C_2H_6\ (+ M) \rightarrow CH_3 + CH_3\ (+ M)$	1.88E+50	–9.72	1.073E+05	7	[42]
Low-pressure limit	3.72E+65	–13.14	1.015E+05		
Troe centering: 0.39	100	1900	6000		
$CH_3COCH_3 + OH \rightarrow CH_3COCH_2 + H_2O$	3.30E+13	0	4.840E+03	8	[32]
$CH_3OH + M \rightarrow CH_3 + OH + M$	5.62E+15	0	6.128E+04	9	[39]

study are effectively independent of the mechanism used, and near-identical results could be obtained using the GRI-Mech 3.0 [21].

TBHP or $(CH_3)_3-CO-OH$) was chosen as an OH radical precursor in the present study, because it decomposes very rapidly to form an OH radical and a tert-butoxy radical, $(CH_3)_3CO$, at temperatures greater than 1000 K [35]. The tert-butoxy radical further decomposes to form acetone and a methyl radical. In addition, TBHP reacts with OH to form other products and the TBHP submechanism was also incorporated into the base mechanism:

$$(CH_3)_3 - CO - OH \rightarrow (CH_3)_3CO + OH \qquad (2)$$

$$(CH_3)_3CO \rightarrow CH_3COCH_3 + CH_3 \qquad (3)$$

$$(CH_3)_3 - CO - OH + OH \rightarrow H_2O + O_2 + \text{tert} - C_4H_9 \qquad (4)$$

$$(CH_3)_3 - CO - OH + OH \rightarrow H_2O + HO_2 + \text{iso} - C_4H_8 \qquad (5)$$

The rate constants for reactions (2), (4), and (5) were adopted from Pang et al. [36], and the rate constant for reaction 3 was obtained from Choo and Benson [37]. The rate constants for reactions (2)–(5) are listed in Table I. In addition, the thermodynamic parameters for TBHP and tert-butoxy radical were taken from the thermodynamic database from Goos et al. [38] and the standard enthalpy of formation for OH radical was updated with the measured value from Herbon et al. [22].

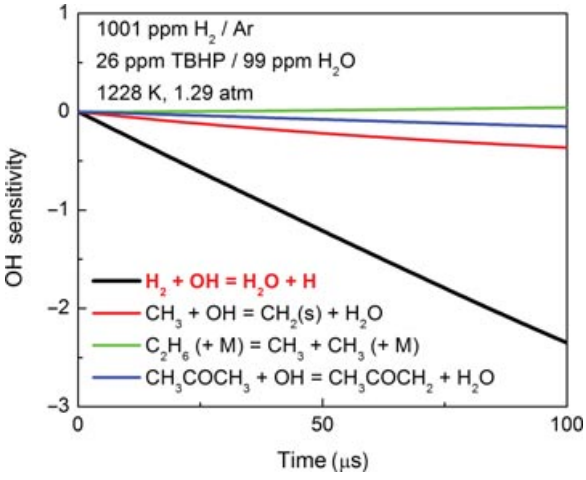

Figure 3 OH sensitivity plot for the rate constant measurement of $H_2 + OH$ at 1228 K and 1.29 atm.

$H_2 + OH$ Kinetics

A local OH sensitivity analysis for the mixture of 1001 ppm H_2 with ~26 ppm TBHP (and 99 ppm H_2O) in Ar at 1228 K and 1.29 atm is shown in Fig. 3. The OH sensitivity is calculated as $S_{OH} = (\partial X_{OH}/\partial k_i) \times (k_i/X_{OH})$, where X_{OH} is the local OH mole fraction and k_i is the rate constant for reaction i. The analysis reveals that the OH time history is predominantly sensitive to the title reaction over the time frame of the experiment, with some minor interference from the following secondary reactions:

$$CH_3 + OH \rightarrow CH_2(s) + H_2O \qquad (6)$$

$$C_2H_6(+ M) \rightarrow CH_3 + CH_3(+ M) \qquad (7)$$

$$CH_3COCH_3 + OH \rightarrow CH_3COCH_2 + H_2O \qquad (8)$$

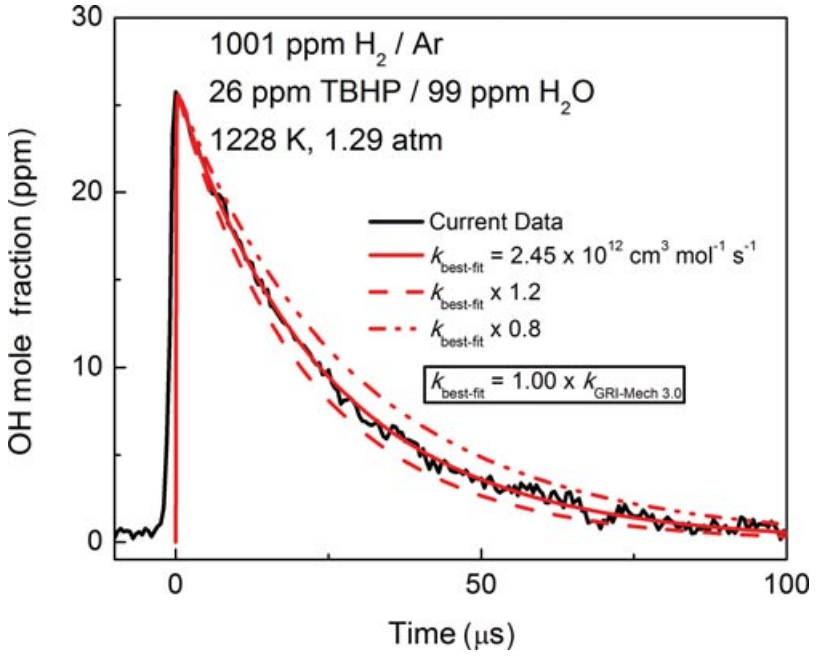

Figure 4 Sample H_2 + OH rate constant measurement using the mixture of 1001 ppm H_2 with ~26 ppm TBHP (and 99 ppm water) in Ar at 1228 K and 1.29 atm. Simulation from USC-Mech v2.0 [34] for the best-fit rate constant, along with perturbations of ±20%, is also shown.

The rate constant for reaction (6) was updated with the value of 1.65×10^{13} cm^3 mol^{-1} s^{-1} recently inferred by Pang et al. [36], which is in good agreement with the measurements from Srinivasan et al. [39] and Vasudevan et al. [40] and the theoretical calculation from Jasper et al. [41] (within ±35%). The rate constant for reaction (7) was updated with the measured values from Oehlschlaeger et al. [42], and the measurements from Oehlschlaeger et al. are in close accord with another experimental study from Kiefer et al. [43]. Recently, Lam et al. [32] have measured the rate constant for reaction (8) using UV laser absorption of OH near 306.69 nm behind reflected shock waves over 872–1355 K at pressures near 2 atm, and their measured rate constant was adopted for reaction (8) in the present study. In addition, the rate constant for the reaction of $CH_3OH + M \rightarrow CH_3 + OH + M$ (reaction (9)) was updated with the measured values from Srinivasan et al. [39] at ~0.3–1.1 atm, and their values agree well with the theoretical calculation from Jasper et al. [41] and the measurements from Vasudevan et al. [40] at 1.3 atm. The rate constants for reactions (6)–(9) are also provided in Table I.

Figure 4 shows an OH time-history measurement for the mixture of 1001 ppm H_2 in argon at 1228 K and 1.29 atm, and the measured peak OH mole fraction is approximately 26 ppm. Owing to wall adsorption and condensation of TBHP, the initial TBHP mole fraction was assumed to be the same as the measured peak OH mole fraction. This assumption is valid because the OH radical is formed very rapidly after the thermal decomposition of TBHP at $T > 1000$ K. More importantly, the presence of H_2O in the mixture has a negligible influence on the simulated OH time history; hence, its presence would not affect our rate constant evaluation. As illustrated in Fig. 4, a best-fit rate constant for reaction (1) of 2.45×10^{12} cm^3 mol^{-1} s^{-1} was obtained between the experimental data and the simulation at 1228 K and 1.29 atm. Simulations for the perturbations of ±20% in the inferred rate constant are also shown in Fig. 4. Similarly, Fig. 5 shows the measured OH time histories for different test mixtures at different temperatures, along with the simulations from USC-Mech v2.0 [34] for the best-fit rate constants. Interestingly, our measured values are identical to or very close to the values originally proposed by Michael and Sutherland [17] within ±4% at most temperatures, and their expression is currently adopted in GRI-Mech 3.0 [21]. In addition, Table II summarizes the rate constant measurements of reaction (1) at $T =$ 902–1518 K and $P = 1.15$–1.52 atm.

A detailed error analysis was performed to estimate the overall uncertainty in the measured rate constant for reaction (1) at 1228 K. The following contributions were considered: (a) temperature (±1%), (b) OH absorption coefficient (±3%), (c) wavemeter reading in

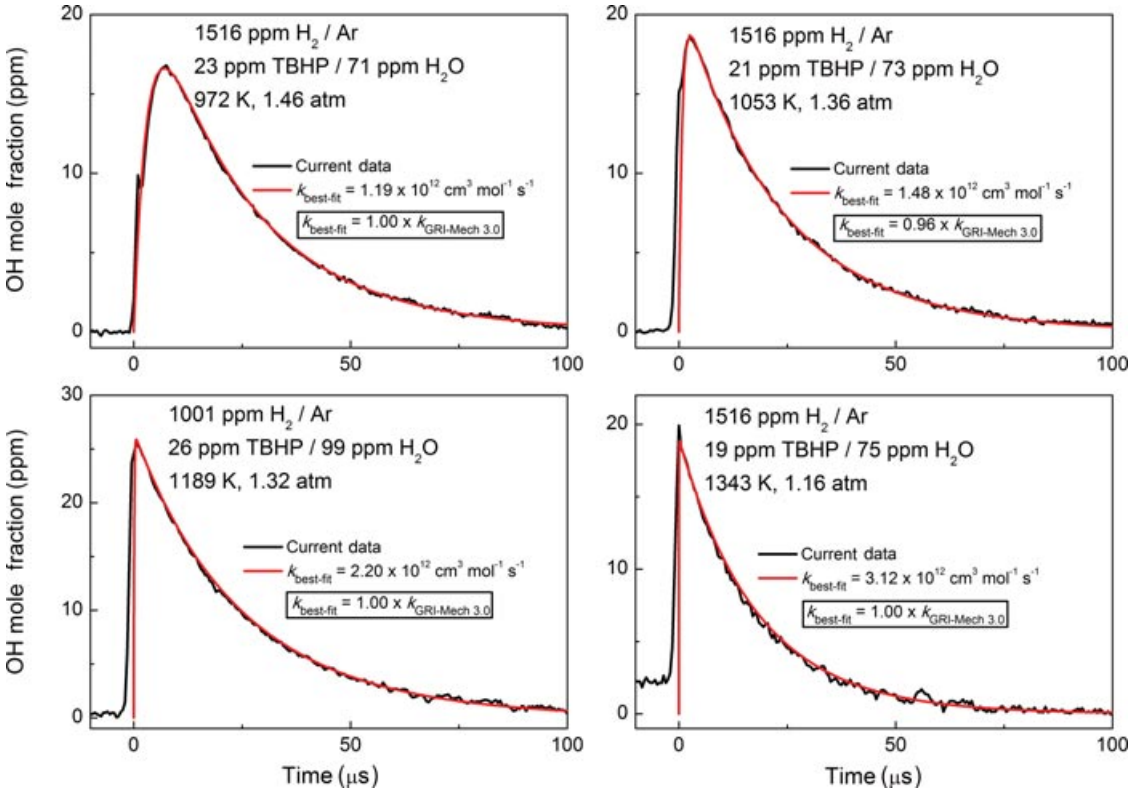

Figure 5 $H_2 + OH$ rate constant measurements at various temperatures, along with the simulations from USC-Mech v2.0 for the best-fit rate constants.

Table II Rate Constant Data for $H_2 + OH \rightarrow H_2O + H$

T_5 (K)	P_5 (atm)	k_1 (cm^3 mol^{-1} s^{-1})
94 ppm TBHP (and water), 1516 ppm H_2, Ar		
1343	1.16	3.12E+12
1053	1.36	1.48E+12
984	1.34	1.31E+12
972	1.46	1.19E+12
933	1.52	1.03E+12
95 ppm TBHP (and water), 1500 ppm H_2, Ar		
1466	1.15	4.10E+12
1405	1.18	3.68E+12
1279	1.23	2.83E+12
1225	1.25	2.38E+12
1217	1.19	2.33E+12
1157	1.30	2.05E+12
1152	1.24	2.03E+12
1140	1.33	1.96E+12
1098	1.35	1.75E+12
981	1.47	1.25E+12
902	1.49	9.23E+11
125 ppm TBHP (and water), 1001 ppm H_2, Ar		
1518	1.15	4.71E+12
1228	1.29	2.45E+12
1189	1.32	2.20E+12
1058	1.43	1.56E+12
1032	1.42	1.40E+12

the UV (± 0.01 cm^{-1}), (d) fitting the data to computed profiles ($\pm 5\%$), (e) locating time-zero (± 0.5 μs), (f) the rate constant for $CH_3 + OH \rightarrow CH_2(s) + H_2O$ (uncertainty factor = 2), (g) the rate constant for C_2H_6 $(+M) \rightarrow CH_3 + CH_3$ $(+M)$ ($\pm 20\%$), and (h) the rate constant for $CH_3COCH_3 + OH \rightarrow CH_3COCH_2 + H_2O$ ($\pm 28\%$). As is evident in Fig. 6, the individual error sources were introduced independently (within the estimated positive and negative bounds of their 2 – σ uncertainties) and their effects on the rate constant for the title reaction were studied. These uncertainties were combined in a root-sum-squared method to give an overall (2 – σ) uncertainty of $\pm 17\%$ at 1228 K. Similar error analysis was conducted for k_1 at 972 K, and the overall (2 – σ) uncertainty was also estimated to be $\pm 17\%$.

Figure 7 shows the Arrhenius plot for the present rate constant measurements of reaction (1) at $T = 902$–1518 K and $P = 1.15$–1.52 atm, along with the non-Arrhenius expression originally proposed by Michael and Sutherland [17]. The measured values from the present study can be expressed in the Arrhenius form as $k_1(T) = 4.38 \times 10^{13} \exp(-3518/T)$ cm^3 mol^{-1} s^{-1} over 902–1518 K. As illustrated in Fig. 7, the current data have a relatively low scatter (<7%). In the present

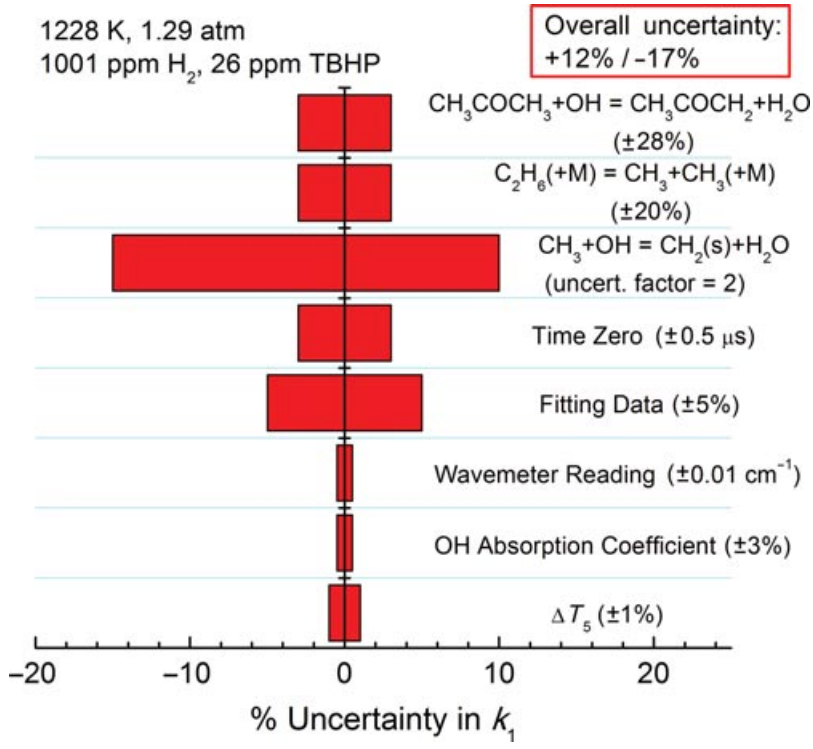

Figure 6 Uncertainty analysis for the rate constant of $H_2 + OH \rightarrow H_2O + H$ at 1228 K and 1.29 atm.

study, three different mixture compositions were utilized to demonstrate that the inferred rate constants are not strongly dependent on any secondary chemistry contributions and the measured values from these mixtures are consistent with each other. It is interesting to note that the present measurements are in excellent agreement with the non-Arrhenius expression proposed by Michael and Sutherland (within ±6%).

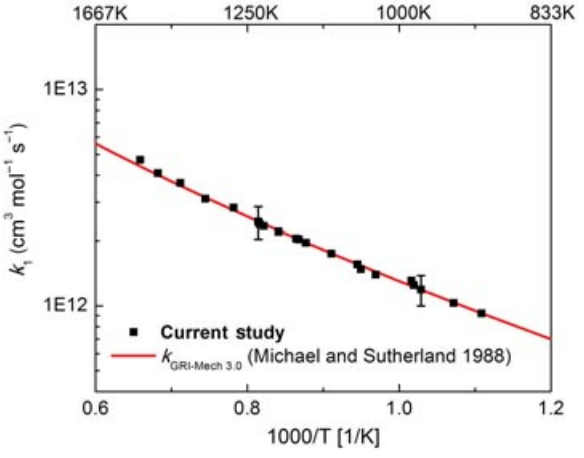

Figure 7 Arrhenius plot for $H_2 + OH$ (k_1) at temperatures above 833 K.

Comparison with Earlier Work

Figure 8 presents the current data along with some earlier measurements of reaction (1) at temperatures above 833 K. Note that the present measurements have a much lower scatter (<7%) than the previous work. Frank and Just [16] investigated the rate constant for reaction (1) using the test mixtures with a few ppm N_2O and 100–500 ppm H_2 and O_2 in Ar behind reflected shock waves over 1700–2500 K. In their experiments, the thermal dissociation of N_2O upon shock heating was used to generate O-atoms, followed by the reaction of $O + H_2 \rightarrow OH + H$ to produce H-atoms and OH radicals. These OH radicals would then react with H_2 through reaction (1), and ARAS was used to monitor H- and O-atom concentration profiles simultaneously. These measured species time histories were also quite sensitive to another major reaction ($H + O_2 \rightarrow OH + O$), which was one of the targeted reactions in their study. Their estimated uncertainty limit for k_1 was found to be less than ±40%. Michael and Sutherland [17] examined the reverse rate constant using the test mixtures of 0.1–1% H_2O in Ar behind reflected shock waves over 1246–2297 K. H-atoms were generated in the postshock regions using the flash photolysis of H_2O and were monitored using ARAS. In the present study, their measured values were also converted to the

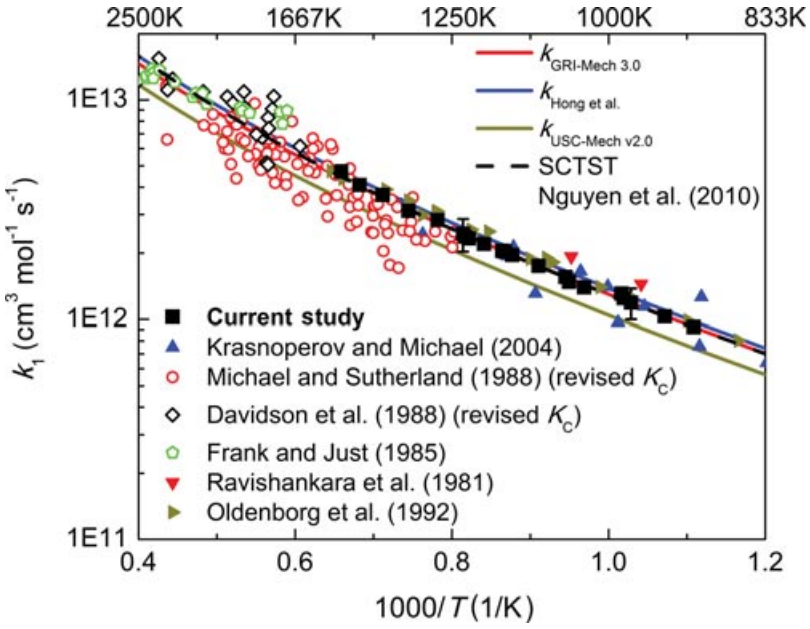

Figure 8 Comparison with previous studies at temperatures above 833 K.

forward rate constants using the revised equilibrium constants (with the revised standard enthalpy of formation for OH from Herbon et al. [22]), as shown in Fig. 8. The new calculated values for reaction (1) are approximately 15% lower than the old values evaluated by Michael and Sutherland. Such differences are solely due to the equilibrium constant evaluations. Nevertheless, their values for reaction (1) have a relatively large experimental scatter (within a factor of 2). Similarly, Davidson et al. [18] measured the reverse rate using the test mixtures of 0.915–1.83% H_2O in Ar behind reflected shock waves over 1600–2500 K. An ArF excimer laser at 193.3 nm was employed to photodissociate a small amount of H_2O to generate H-atoms and OH radicals, and a cw, narrow-linewidth ring dye laser at 306.6 nm was then used to monitor the temporal evolution of OH radicals. The errors of their measurements varied from ±40% at 1600 K to ±12% at 2500 K. Their measured values were also converted to the forward rates using the revised equilibrium constants. As illustrated in Fig. 8, the data from Frank and Just [16], Michael and Sutherland [17], and Davidson et al. [18] are in good agreement with each other (within their experimental scatter). Oldenborg et al. [19] also conducted direct rate constant measurements of reaction (1) using the laser photolysis/heated flow cell technique and using laser-induced fluorescence method to monitor the temporal profiles of OH decays at 800–1550 K. Their experiments were performed under pseudo–first-order kinetic conditions with an excess of H_2. In addition, Ravishankara et al. [8] studied reaction (1) using the flash photolysis–resonance fluorescence technique (under pseudo–first-order kinetic conditions) in a heated quartz cell over 250–1050 K and their high-temperature measurements (at 960 and 1050 K) are ∼20% higher than the measurements from Oldenborg et al. [19]. Moreover, Krasnoperov and Michael [20] re-examined reaction (1) using a test mixture of ∼5 ppm TBHP with 404 ppm H_2 in krypton behind reflected shock waves at lower temperatures (832–1359 K). TBHP was utilized as the OH precursor in their study, and a novel multipass absorption spectrometric detection method (with a MW discharge driven resonance OH lamp) was employed to measure OH species profiles. Although their experimental scatter is slightly high (±25%), their measured values are generally in good agreement with Oldenborg et al. [19] and Ravishankara et al. [8]. Concurrently, the present measurements are in excellent agreement with all previous studies.

Figure 8 also shows the values of k_1 employed in three different comprehensive reaction mechanisms: GRI-Mech 3.0 [21], USC-Mech v2.0 [34], and Hong et al. [44]. The present measurements agree well with the values from GRI-Mech 3.0 and Hong et al. (within ±6%). However, the values of k_1 from USC-Mech v2.0 are ∼20% lower than the present measurements. Concurrently, Nguyen et al. [45] computed the rate constant for the title reaction with semiclassical transition state theory (SCTST), which implemented

nonseparable coupling among all degrees of freedom (including the reaction coordinate) in the transition state region and multidimensional quantum mechanical tunneling along the curved reaction path. Their theoretical calculation (the black dashed line in Fig. 8) is also in excellent agreement with the present and previous experimental studies, and their calculation is nearly indistinguishable from the rate constant adopted in GRI-Mech 3.0.

CONCLUSIONS

The rate constant for the reaction of $H_2 + OH \rightarrow H_2O + H$ was studied behind reflected shock waves over the temperature range of 902–1518 K at pressures of 1.15–1.52 atm using OH laser absorption. The current high-temperature data can be expressed in the Arrhenius equation as $k_1(T) = 4.38 \times 10^{13} \exp(-3518/T)$ $cm^3\ mol^{-1}\ s^{-1}$ over the temperature range studied. A detailed error analysis was carried out with the consideration of both experimental and secondary chemistry contributions, and the overall $(2 - \sigma)$ uncertainties in k_1 were found to be $\pm 17\%$ at 972 and 1228 K. Note that the experimental scatter from the present study is less than 7%, which is much lower than the previous work [16–20]. The present data are consistent with the previous measurements from Frank and Just [16], Michael and Sutherland [17], Davidson et al. [18], Oldenborg et al. [19], and Krasnoperov and Michael [20]. In addition, the present measurements are in excellent agreement with the non-Arrhenius expression from GRI-Mech 3.0 [21] and the recent theoretical calculation using SCTST from Nguyen et al. [45].

The authors would like to acknowledge Robert Cook for his assistance with laboratory equipment during experiments. Prof. Hai Wang is also acknowledged for sharing the flame speed simulations from his preliminary CEFRC foundational fuel model. This work was supported by the U.S. Department of Energy, Basic Energy Sciences (DE-FG02-88ER13857) with Dr. Wade Sisk as program manager and was also supported by the National Science Foundation (NSF ENG/CBET) under award no. 0964884.

BIBLIOGRAPHY

1. Kaufman, F.; Del Greco, F. P. Symp (Int) Combust 1963, 9, 659–668.
2. Dixon-Lewis, G.; Wilson, W. E.; Westenberg, A. A. J Chem Phys 1966, 44, 2877–2884.
3. Greiner, N. R. J Chem Phys 1967, 46, 2795–2799.
4. Greiner, N. R. J Chem Phys 1969, 51, 5049–5051.
5. Stuhl, F.; Niki, H. J Chem Phys 1972, 57, 3671–3677.
6. Westenberg, A. A.; deHaas, N. J Chem Phys 1973, 58, 4061–4065.
7. Tully, F. P.; Ravishankara, A. R. J Phys Chem 1980, 84, 3126–3130.
8. Ravishankara, A. R.; Nicovich, J. M.; Thompson, R. L.; Tully, F. P. J Phys Chem 1981, 85, 2498–2503.
9. Talukdar, R. K.; Gierczak, T.; Goldfarb, L.; Rudich, Y.; Rao, B. S. M.; Ravishankara, A. R. J Phys Chem 1996, 100, 3037–3043.
10. Smith, I. W. M.; Zellner, R. J Chem Soc, Faraday Trans 2 1974, 70, 1045–1056.
11. Overend, R. P.; Paraskevopoulos, G.; Cvetanovic, R. J. Can J Chem 1975, 53, 3374–3382.
12. Atkinson, R.; Hansen, D. A.; Pitts, J. N., Jr. J Chem Phys 1975, 62, 3284–3288.
13. Atkinson, R.; Hansen, D. A.; Pitts, J. N., Jr. J Chem Phys 1975, 63, 1703–1706.
14. Orkin, V. L.; Kozlov, S. N.; Poskrebyshev, G. A.; Kurylo, M. J. J Phys Chem A 2006, 110, 6978–6985.
15. Gardiner, W. C., Jr.; Mallard, W. G.; Owen, J. H. J Chem Phys 1974, 60, 2290–2295.
16. Frank, P.; Just, Th. Ber Bunsen-Ges Phys Chem 1985, 89, 181–187.
17. Michael, J. V.; Sutherland, J. W. J Phys Chem 1988, 92, 3853–3857.
18. Davidson, D. F.; Chang, A. Y.; Hanson, R. K. Symp (Int) Combust 1988, 22, 1877–1885.
19. Oldenborg, R. C.; Loge, G. W.; Harradine, D. M.; Winn, K. R. J Phys Chem 1992, 96, 8426–8430.
20. Krasnoperov, L. N.; Michael, J. V. J Phys Chem A 2004, 108, 5643–5648.
21. Smith, G. P.; Golden, D. M.; Frenklach, M.; Moriarty, N. W.; Eiteneer, B.; Goldenberg, M.; Bowman, C. T.; Hanson, R. K.; Song, S.; Gardiner, W. C., Jr.; Lissianski, V. V.; Qin, Z. http: //www.me.berkeley.edu/gri_mech/. Accessed 30 July 1999.
22. Herbon, J. T.; Hanson, R. K.; Golden, D. M.; Bowman, C. T. Proc Combust Inst 2002, 29, 1201–1208.
23. Tse, S. D.; Zhu, D. L.; Law, C. K. Proc Combust Inst 2000, 28, 1793–1800.
24. Dowdy, D. R.; Smith, D. B.; Taylor, S. C.; Williams, A. Symp (Int) Combust 1990, 23, 325–332.
25. Aung, K. T.; Hassan, M. I.; Faeth, G. M. Combust Flame 1997, 109, 1–24.
26. Egolfopoulos, F. N.; Law, C. K. Symp (Int) Combust 1990, 23, 333–340.
27. Lamoureux, N.; Djebayli-Chaumeix, N.; Paillard, C.-E. Exp Therm Fluid Sci 2003, 27, 385–393.
28. Huang, Z.; Zhang, Y.; Zeng, K.; Liu, B.; Wang, Q.; Jiang, D. Combust Flame 2006, 146, 302–311.
29. Tang, C.; Huang, Z.; Jin, C.; He, J.; Wang, J.; Wang, X.; Miao, H. Int J Hydrogen Energy 2008, 33, 4906–4914.
30. Hu, E.; Huang, Z.; He, J.; Jin, C.; Miao, H.; Wang, X. Chin Sci Bull 2009, 54, 846–857.
31. Wang, H. Private communication, August 2012.
32. Lam, K.-Y.; Davidson, D. F.; Hanson, R. K. J. Phys. Chem. A 2012, 116, 5549–5559.
33. Chemkin PRO Release 15101; Reaction Design: San Diego, CA, 2010.

34. Wang, H.; You, X.; Joshi, A. V.; Davis, S. G.; Laskin, A.; Egolfopoulos, F.; Law, C. K. USC-Mech Version II. High-Temperature Combustion Reaction Model of H2/CO/C1–C4 Compounds. Available at http: ignis.usc.edu/USC_Mech_II.htm. Accessed May 2007.
35. Benson, S. W.; O'Neal, H. E. Kinetic Data on Gas Phase Unimolecular Reactions; NSRDS-NBS 21; National Bureau of Standards: Washington, DC, 1970.
36. Pang, G. A.; Hanson, R. K.; Golden, D. M.; Bowman, C. T. Z Phys Chem 2011, 225, 1157–1178.
37. Choo, K. Y.; Benson, S. W. Int J Chem Kinet 1981, 13, 833–844.
38. Goos, E.; Burcat, A.; Ruscic, B. Third Millennium Ideal Gas and Condensed Phase Thermochemical Database for Combustion, May 30, 2011. Available at http://garfield.chem.elte.hu/Burcat/burcat.html.
39. Srinivasan, N. K.; Su, M.-C.; Michael, J. V. J Phys Chem A 2007, 111, 3951–3958.
40. Vasudevan, V.; Cook, R. D.; Hanson, R. K.; Bowman, C. T.; Golden, D. M. Int J Chem Kinet 2008, 40, 488–495.
41. Jasper, A. W.; Klippenstein, S. J.; Harding, L. B.; Ruscic, B. J Phys Chem A 2007, 111, 3932–3950.
42. Oehlschlaeger, M. A.; Davidson, D. F.; Hanson, R. K. Proc Combust Inst 2005, 30, 1119–1127.
43. Kiefer, J. H.; Santhanam, S.; Srinivasan, N. K.; Tranter, R. S.; Klippenstein, S. J.; Oehlschlaeger, M. A. Proc Combust Inst 2005, 30, 1129–1135.
44. Hong, Z.; Davidson, D. F.; Hanson, R. K. Combust Flame 2011, 158, 633–644.
45. Nguyen, T. L.; Stanton, J. F.; Barker, J. R. Chem Phys Lett 2010, 499, 9–15.